An AIMD study of dissociative chemisorption of methanol on Cu(111) with implications for formaldehyde formation

Nick Gerrits[1, a)] and Geert-Jan Kroes[1, b)]

Leiden Institute of Chemistry, Leiden University, Gorlaeus Laboratories,
P.O. Box 9502, 2300 RA Leiden, the Netherlands

(Dated: December 13, 2018)

An important industrial process is methanol steam reforming, which is typically used in conjunction with copper catalysts. However, little agreement exists on the reaction mechanisms involved on a copper catalyst. Therefore, we have performed research yielding additional insight into the reaction mechanism for dissociative chemisorption of methanol on Cu(111) using ab initio molecular dynamics (AIMD), supported by static calculations of the molecule-surface interaction with DFT. Our work predicts that after the initial dissociation formaldehyde is formed, through three different mechanisms. Additionally, it is observed that at high energy CH cleavage is the dominant pathway instead of the formerly presumed OH cleavage pathway. Finally, in order to describe the interaction of methanol with the metal surface, the SRP32-vdW functional is used, which has been previously developed and tested for CHD_3 on Ni(111), Pt(111) and Pt(211) using the Specific Reaction Parameter approach (SRP). In this work the SRP32-vdW functional is applied to methanol on Cu(111) as well, in the hope that future experiments can validate the transferability of the SRP32-vdW functional to chemically related molecule-metal surface systems.

---

a)Electronic mail: n.gerrits@lic.leidenuniv.nl
b)Electronic mail: g.j.kroes@chem.leidenuniv.nl

I. INTRODUCTION

Methanol steam reforming is an important industrial process with several applications such as formaldehyde and syngas production. However, there is little agreement concerning the reaction mechanisms of methanol on metal surfaces, especially on copper-based catalysts[1]. Due to the existence of several different chemical bonds, methanol dissociation is described by a complex reaction scheme involving several products being formed via different pathways. Furthermore, little is known about the mechanisms that follow the breaking of the first bond in methanol. For example, experimental evidence for formaldehyde formation on copper catalysts through direct decomposition of methanol exists[2–5], although the underlying pathways remain unclear. So far, theoretical calculations have only been able to deal with this reaction scheme on a static level using transition state theory[6–12] or a dynamical level but with a frozen surface[13]. However, these levels of theory exclude exchange of energy between the surface and the molecule and transition state theory excludes any dynamical effects such as steering as well. Moreover, although the complete steam reforming reaction of methanol to CO_2 and hydrogen of course also involves water, water only plays a role after the initial reaction steps, i.e. after formaldehyde is formed, by hydrolyzing either a methyl formate intermediate or formaldehyde[1]. Depending on the reaction conditions, the preceding formation of formaldehyde is often the rate controlling step for methanol steam reforming[14–17], and thus an important reaction step to investigate. Therefore, in this work water is neglected and only the dissociative chemisorption of methanol and subsequent formation of formaldehyde on Cu(111) is investigated using ab initio molecular dynamics (AIMD) in order to include dynamical effects. Finally, on Pt(111) and Ru(0001) the methanol decomposition mechanism can be affected by the methanol pre-coverage, while no such dependence has been reported on Cu(111), on which methanol has a lower adsorption energy[9]. Since our simulations are performed in the zero coverage limit, i.e. only initial sticking of methanol on a clean surface is considered, our results should therefore be relevant for catalysis at sufficiently low pressure and sufficiently high temperatures.

Moreover, to model accurately the interaction between molecules and metal surfaces remains challenging[18–22]. Therefore, the Specific Reaction Parameter (SRP) approach has been used to develop a chemically accurate functional (SRP32-vdW) for methane on Ni(111), Pt(111) and Pt(211)[23,24]. The SRP32-vdW functional was first developed for CHD_3 +

Ni(111)[23]) and later shown to be transferable to methane interacting with metals within the same periodic table group (CHD_3 + Pt(111)[24]) and to stepped surfaces (CHD_3 + Pt(211)[24,25]). Here we have performed predictive calculations on methanol, which is chemically related to methane, and on a metal surface belonging to a neighbouring group of the periodic table. We hope that our predictions will be followed by experiments in order to validate the transferability of the SRP32-vdW functional to methanol on a Cu(111) surface.

To summarize, this work makes a prediction for the reactivity of methanol on Cu(111), combined with a detailed analysis of the dynamical behaviour. Furthermore, new insights are gained for the reaction mechanisms for the formation of formaldehyde on Cu(111). The paper is structured as follows: a short summary of the technical details is given in Section II. Moreover, the barriers and elbow plots obtained with static DFT calculations are discussed in Sections III A and III B. In Section III C the reaction probabilities are presented, followed by the impact site associated with reactive collisions in Section III D. Furthermore, Section III E concerns the energy transfer of methanol to the surface, and Section III F the orientations methanol goes through during the reaction. Finally, formaldehyde formation is discussed in Section III G, and a short summary is given in Section IV.

II. METHOD

The Vienna Ab-initio Simulation Package (VASP version 5.3.5)[26–30] is used for the AIMD and electronic structure (Density Functional Theory, DFT) calculations. A kinetic energy cutoff of 400 eV and a Γ-centered 3x3x1 k-point grid are used. Moreover, core electrons have been represented with the Projector Augmented Wave method (PAW)[30,31]. The surface is modeled using a 4 layer (4x3) supercell, where the angle between the x and y vectors is 30 degrees instead of the usual 60 degrees, i.e. a skewed unit cell is used. Furthermore, a vacuum distance of 15 Å is used between the slabs and the top three layers have been relaxed in the z direction. In order to speed up convergence, first order Methfessel-Paxton smearing[32] with a width parameter of 0.2 eV has been applied. Convergence of the employed computational setup is confirmed to be within chemical accuracy (1 kcal/mol, or 4.2 kJ/mol) and results connected to this convergence are given in the supporting information.

Transition states are obtained with the dimer method[33–36] as implemented in the VASP Transition State Tools package (VTST), and are confirmed to be first order saddle points

Table I. Experimental beam parameters that describe the simulated methanol velocity distributions. ν_0 and α are determined through time-of-flight measurements for 600, 750 and 900 K[23]. The parameters for $\langle E_i \rangle = 163.1$ kJ/mol are not from experiment, but theoretical estimates obtained by extrapolation.

T_n (K)	$\langle E_i \rangle$ kJ/mol	ν_0 (m/s)	α (m/s)
500*	163.1	3177.70	158.89
600	188.7	3418.09	168.02
750	229.2	3760.72	216.91
900	269.5	4070.12	274.51

by checking if only one imaginary frequency is found at the transition state. Forces on the degrees of freedom are converged within 5 meV/Å, where the degrees of freedom are for the motion of the methanol atoms.

For the AIMD simulations a surface temperature of 550 K is used, where the atoms in the top three layers are allowed to move in all three directions and the ideal lattice constant is expanded by a factor of 1.0078 in order to reflect the expansion of the bulk due to the surface temperature[37]. Methanol molecular beam bundles were simulated according to the parameters in Table I, which were obtained for CHD_3 seeded in H_2 molecular beam bundles in Ref.[23]. It is assumed that methanol has a similar velocity slip in a molecular beam as methane, hence beam parameters obtained for CHD_3 are used here for methanol. For every AIMD data point, 500 trajectories were run, with a time step of 0.4 fs. The rest of the technical details of the AIMD calculations can be found in recent work[23,24,38,39] and in the supporting information. We use the SRP32-vdW functional previously used for CHD3 + Ni(111), Pt(111), Pt(211), Cu(111) and Cu(211)[23,24,39], of which the exchange part is defined as

$$E_x = x \cdot E_x^{RPBE} + (1-x) \cdot E_x^{PBE}, \qquad (1)$$

where E_x^{RPBE} and E_x^{PBE} are the exchange parts of the RPBE and PBE[40,41] exchange-correlation functionals, respectively, and $x = 0.32$. Moreover, for the correlation part the vdW correlation functional of Dion and coworkers (vdW-DF1)[42] is used.

Table II. The barrier geometries for methanol on Cu(111). The labels indicate whether OH or CH cleavage occurred and the location of the broken bond. Zero-point energy corrected barriers are given in the brackets.

Label	$Z_C^\ddagger$(Å)	$Z_O^\ddagger$(Å)	$r^\ddagger$(Å)	$\theta^\ddagger$(deg)	$\beta^\ddagger$(deg)	$\gamma 1^\ddagger$(deg)	$\gamma 2^\ddagger$(deg)	$\alpha^\ddagger$(deg)	$\phi^\ddagger$(deg)	E_b (kJ/mol)
OH-fcc1	3.06	1.89	1.62	117.8	144.4	64.9	63.9	144.3	1.0	92.4 (75.7)
OH-bridge1	3.11	1.75	1.49	112.5	158.9	59.3	59.6	159.2	0.4	95.1 (78.1)
CH-top1	2.46	2.85	2.03	132.5	110.6	138.0	24.7	73.5	130.3	130.4 (116.2)
CH-top2	2.46	2.87	2.02	134.5	111.8	135.3	24.4	72.5	130.0	130.4 (116.4)

III. RESULTS

A. Barriers

The obtained barrier geometries for methanol on Cu(111) are summarized in Figure 1 and Table II. Additionally, the θ, γ_1, α and ϕ angles used to describe the transition state geometries in Table II are depicted in Figure 2. θ is the angle between the surface normal and the dissociating OH or CH bond and β denotes the angle between the surface normal and the umbrella axis, which is defined as the vector going through the geometric center of the three H-atoms and the carbon. Furthermore, γ_1 defines the angle between the CO bond and the dissociating CH or OH bond, whereas γ_2 defines the angle between the umbrella axis and the dissociating CH or OH bond. Finally, α describes the angle between the CO bond and surface normal and ϕ indicates the angle between the umbrella axis and the CO bond.

The lowest barrier height found is the OH-fcc1 geometry, where the OH bond is broken above the fcc site. The barrier height of this geometry is 92.4 kJ/mol, which is in good agreement with earlier results[9]. Another barrier for OH cleavage is found above the bridge site (OH-bridge1), which is 2.6 kJ/mol higher than the OH-fcc1 barrier. Both barrier geometries are similar, except for the larger dissociating bond length and tilt of the molecule w.r.t. the surface normal (i.e. β is larger) of the OH-fcc1 geometry compared to OH-bridge1.

Furthermore, the barrier height found for CH cleavage is considerably higher than OH cleavage (38 kJ/mol higher). The two obtained barriers for CH cleavage have identical barrier heights (130.4 kJ/mol) and similar geometries, where the major difference is the orientation

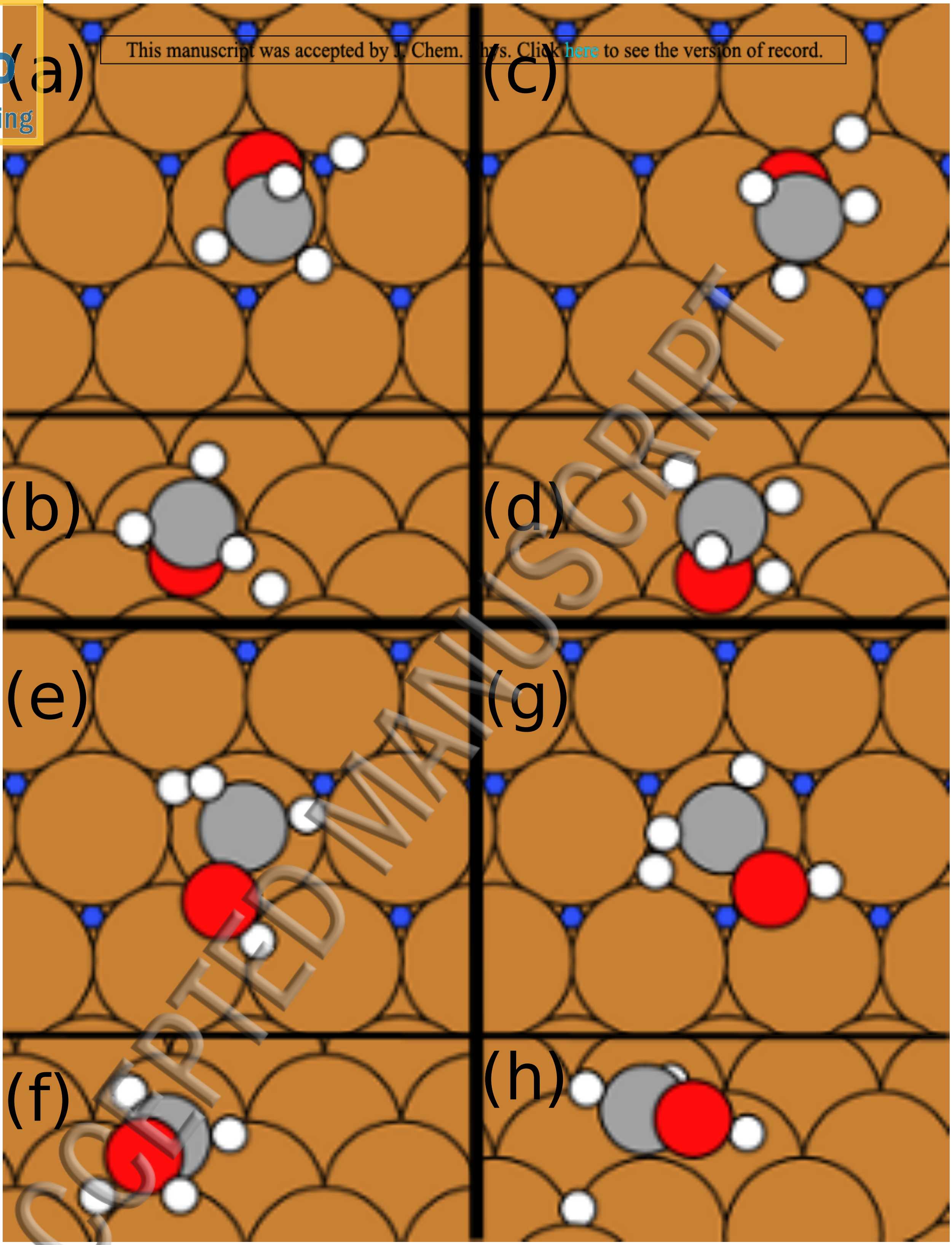

Figure 1. Top and side view of the transition state of methanol on Cu(111) with the OH-fcc1 (a,b), OH-bridge1 (c,d), CH-top1 (e,f), and CH-top2 (g,h) geometries. At the surface, blue circles indicate the fcc sites.

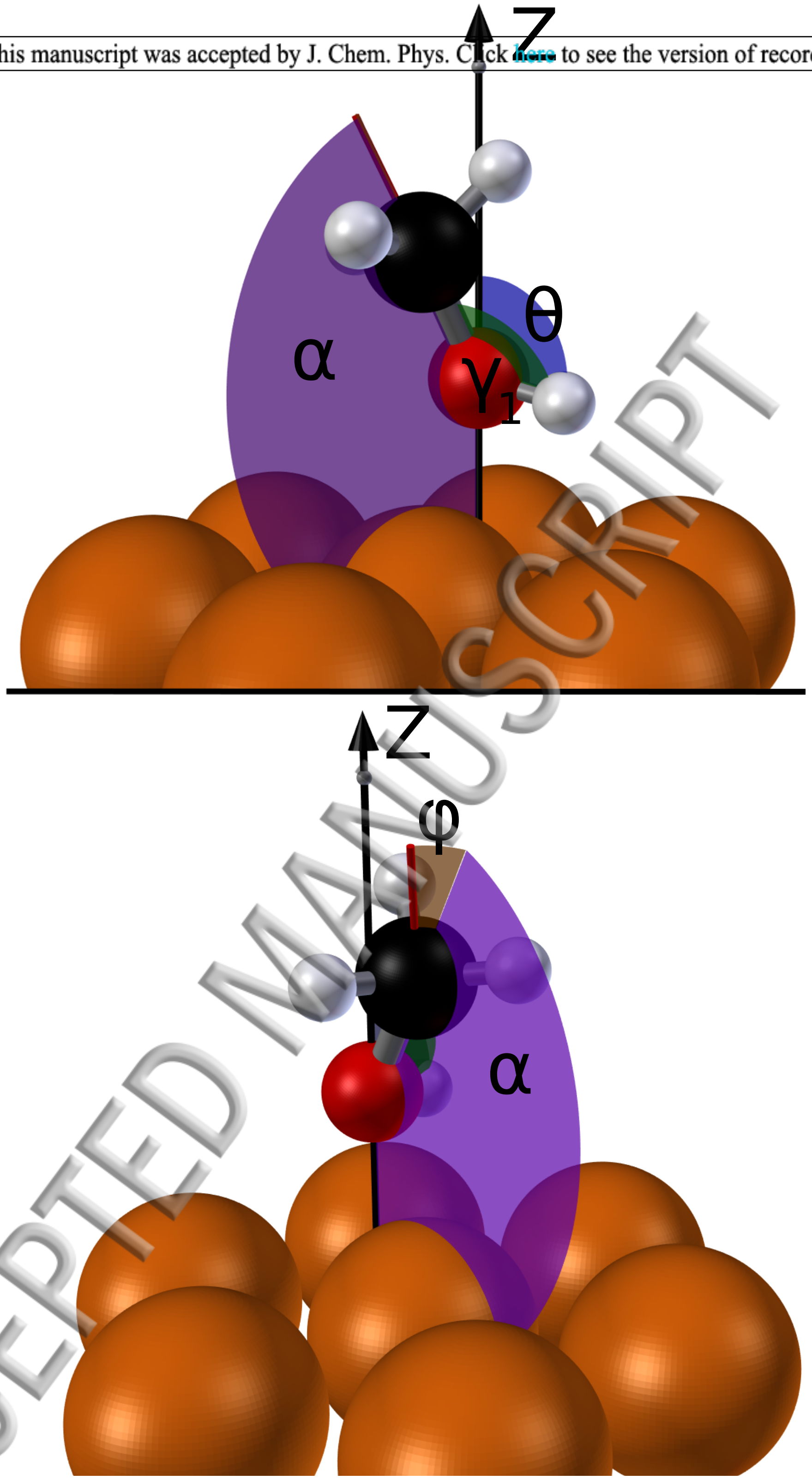

Figure 2. The θ, γ_1, α and ϕ angles used to describe the methanol geometry.

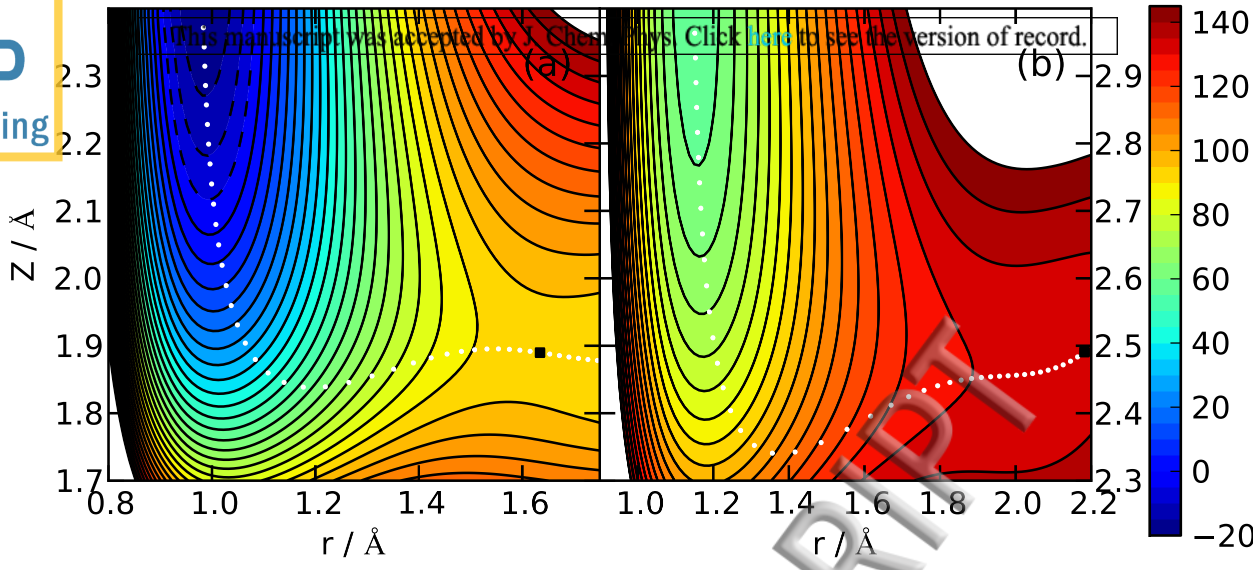

Figure 3. Elbow plot of methanol on Cu(111), where methanol is fixed in it the OH-fcc1 (a) or CH-top1 (b) transition state geometry, whereas Z and the bond length of the dissociating hydrogen are variable. Contour lines are drawn at intervals of 5 kJ/mol between -20 and 150 kJ/mol. The colours indicate the energy (kJ/mol) w.r.t. methanol in the gas phase and the black squares indicate the highest point along the MEP.

of the molecule w.r.t. the high-symmetry sites. Moreover, the barrier for CH cleavage is considerably later than for OH cleavage due to the larger dissociating bond length. From both a dynamical and energetic point of view this would mean that the minimum barrier for OH cleavage is more easily accessible than for CH cleavage. Also, in the barrier geometries for OH cleavage the CO bond is perpendicular to the surface, whereas in the geometries for CH cleavage the CO bond is parallel to the surface. Finally, no barrier is obtained for CO cleavage, but it is expected to be considerably higher than the barriers obtained in this work[9].

B. Minimum energy path

Figure 3 shows the elbow plots for the OH-fcc1 and CH-top1 barriers, where methanol is kept fixed in its transition state geometry while varying Z and the bond length of the dissociating hydrogen. Z is defined as the distance between the surface and oxygen for the

OH-fcc1 barrier and between the surface and carbon for the CH-top1 barrier. The OH-fcc1 barrier is earlier (i.e. the dissociating bond length is smaller) and closer to the surface than the CH-top1 barrier, as also evident from the aforementioned barrier geometries in Table II. Furthermore, the minimum energy path (MEP) of the OH-fcc1 barrier is less curved than the MEP of the CH-top1 barrier. This could imply that the OH-fcc1 barrier is not only more accessible than the CH-top1 barrier from a barrier height point of view, but also from a dynamical point of view in connection with the "*bobsled effect*"[43,44]. Finally, elbow plots have not been obtained for other barrier geometries, however, similar results are expected.

C. Sticking probability

A prediction for the reactivity of methanol on Cu(111) using AIMD is presented in Figure 4. The vibrational efficacy of exciting the OH stretch mode ($\nu_1 = 1$) is very high compared to the laser off predictions (about 2). Furthermore, exciting the OH stretch mode suppresses CH cleavage, while for laser off experiments a higher fraction of CH cleavage is predicted at higher incidence energies. Also, at $\langle E_i \rangle = 270$ kJ/mol about 0.5% of the reacted trajectories were due to CO cleavage, which can be expected due to the very high kinetic energy of methanol at these incidence energies, which exceeds even the high barrier height for CO cleavage[9]. Finally, trapping is observed as well, however, due to the timescales involved with trapping it is not possible to obtain statistical data for a reaction probability including a trapping mechanism, i.e. only an upper bound for King and Wells experiments[45] can be given.

D. Reaction site

The distribution of the distance of reacting methanol (only the reactions involving OH cleavage) to the high symmetry sites is given in Figure 5 and compared to the statistical distributions. In general, no steering is observed for the methanol in the x and y directions. Furthermore, as can be seen in Figure 6, for the vibrationally excited results the distance to the high symmetry sites is statistical. However, at lower incidence energy with the laser off, methanol is more likely to react closer to the hollow and bridge sites instead of the top site. This could mean that methanol does not react over the minimum OH cleavage barrier

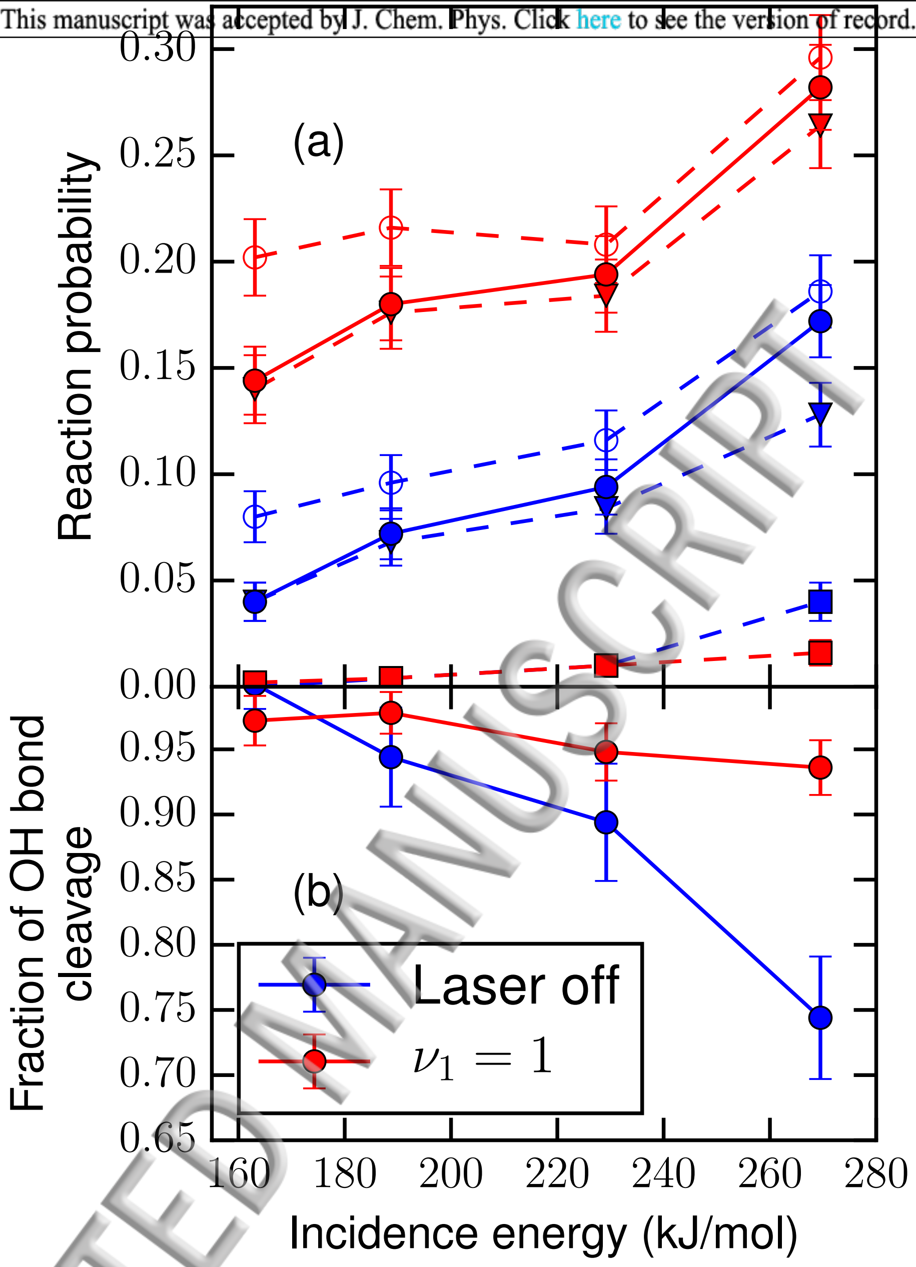

Figure 4. Reaction probability of methanol on Cu(111) for laser off (blue) and $\nu_1 = 1$ (red) AIMD simulations (a), and the fraction of reactions that occurred through OH bond cleavage (b). In panel A, squares and triangles indicate dissociation of the CH and OH bond, while the solid circles indicate the total dissociation probability and open circles also include trapping. The error bars represent 68% confidence intervals.

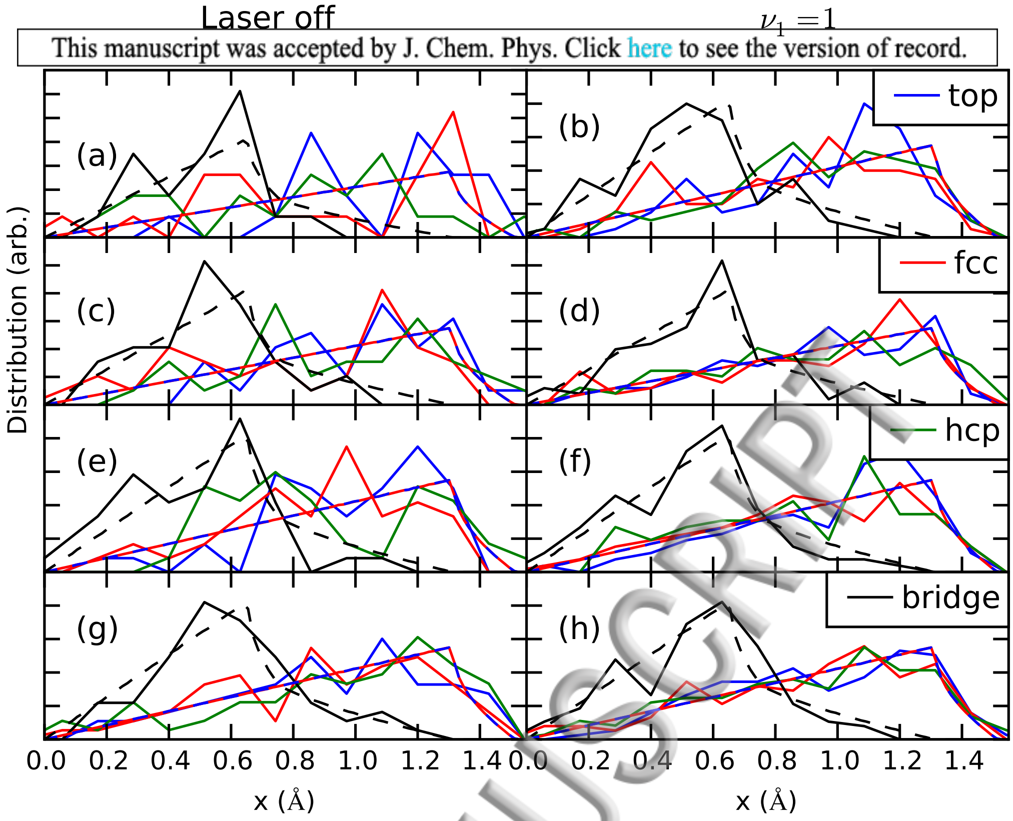

Figure 5. The distributions of the distance (Å) of the reacting methanol (through OH cleavage) to the closest top (blue), fcc (red), hcp (green) and bridge (black) sites on Cu(111) for laser off (a,c,e,g) and $\nu_1 = 1$ (b,d,f,h), with $\langle E_i \rangle = 163$ (a,b), $\langle E_i \rangle = 189$ (c,d), $\langle E_i \rangle = 229$ (e,f) and $\langle E_i \rangle = 270$ (g,h) kJ/mol. The blue and red dashed line indicates the statistical distribution for the hollow and top sites, while the black dashed line is the statistical distribution for the bridge site.

(OH-fcc1), for which the center of mass of methanol would be above the top site, but rather via the OH-bridge1 barrier above the hollow or bridge site. This could be possible due to the fact that the OH-bridge1 barrier height is only 2.6 kJ/mol higher than the OH-fcc1 barrier height. Furthermore, the OH-bridge1 barrier is earlier than the OH-fcc1 barrier and thus it would be dynamically more accessible. Finally, due to the small amount of trajectories leading to CH or CO cleavage, no conclusions can be drawn regarding the differences between the site specificity for CH and CO cleavage. However, it does seem that at lower energies CH cleavage happens more closely to the top site, which again can be expected from the minimum barrier.

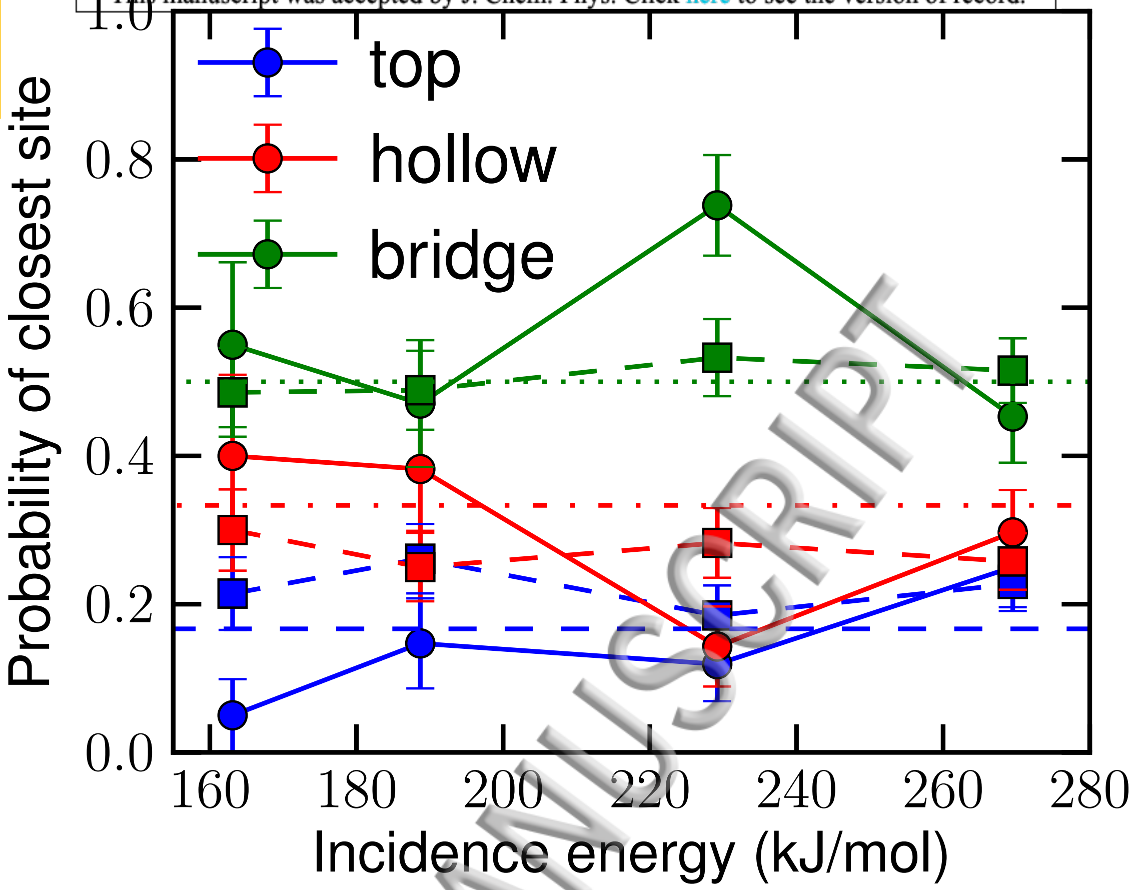

Figure 6. The fraction of closest high symmetry site to the impact site of reacting methanol on Cu(111) for laser off (solid lines with circles) and $\nu_1 = 1$ (dashed lines with squares) compared to the incidence energy. The dotted green line indicates the statistical average for the bridge site, whereas the dashed and dotted red line indicates the statistical average for the hollow sites. The dashed blue line is the statistical average for the top site. The error bars represent 68% confidence intervals.

E. Energy transfer to the surface

The average energy transfer of scattered methanol to the surface using AIMD and predicted by the corrected Baule model[46,47] are compared in Figure 7. The formula for the corrected Baule model is $E_T = \langle E_i \rangle \, 2.4\mu/(1+\mu)^2$, where $\mu = m/M$ (with m as the mass of the projectile and M as the mass of a surface atom) and γ is the angle between the velocity

AIP Publishing

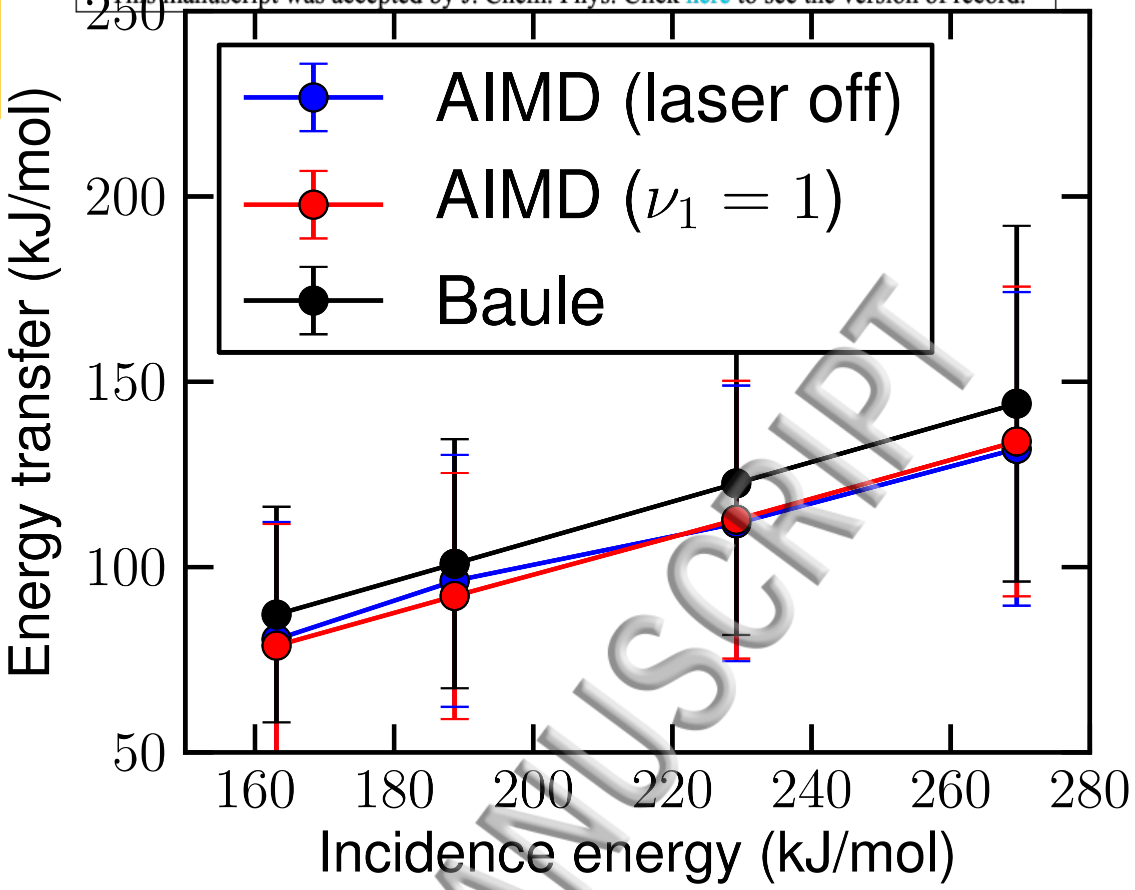

Figure 7. Energy transfer from scattered methanol to the surface for laser off and $\nu_1 = 1$ AIMD simulations, and corrected Baule model[46,47] at various incidence energies. The error bars represent 68% confidence intervals.

vector of the molecule and the line connecting the centers of the hard spheres at impact. Here we see that the Baule model is in remarkably good agreement with AIMD. Half of the translational energy is transferred to the surface, which is due to the small mass difference between a Cu surface atom and the methanol molecule. Due to this large energy transfer of methanol to the surface, it is expected that surface atom motion plays a considerable role in the reactivity of methanol on Cu(111).

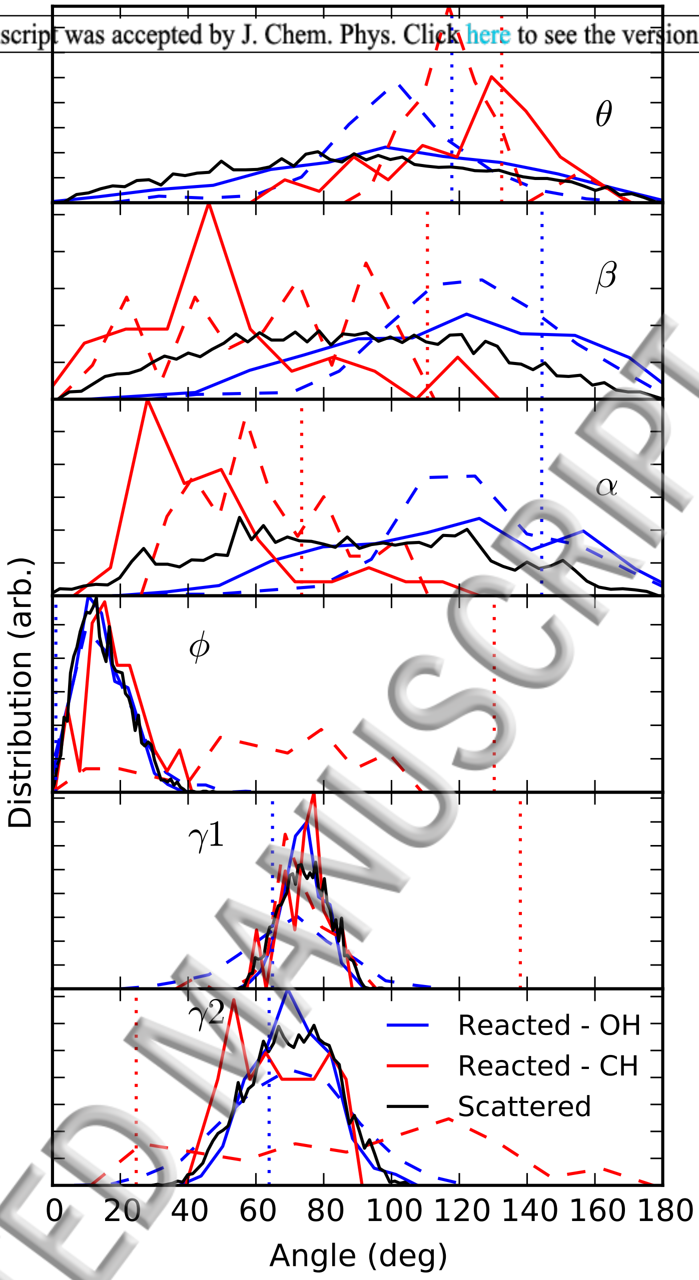

Figure 8. Angular distributions describing the orientation of methanol during AIMD for scattered (black) and reacted trajectories at the initial time step (solid lines) and when a dissociating bond reaches the transition state value (dashed lines). Results for all incidence energies, and laser off and on are combined. The blue lines indicate OH cleavage, while the red lines indicate CH cleavage. The dotted lines represent the transition state values for the OH-fcc1 (blue) and CH-top1 (red) geometries.

F. Angular distributions

Angular distributions of methanol extracted from the AIMD simulations are shown in Figure 8. θ indicates the orientation of the dissociating bond, whereas β and α indicate the orientation of the umbrella axis and the CO bond, respectively. Furthermore, ϕ concerns the angle between the CO bond and the umbrella axis, and γ_1 and γ_2 are the angles of the CO bond and umbrella axis w.r.t. the dissociating bond. For the initial values, i.e. at $t = 0$ fs, no differences were found between scattered and reacted trajectories in the ϕ and γ angles. However, for the θ, β and α angles differences are found not only between scattered and reacted trajectories, but also between OH and CH cleavage. These differences can be explained by the differences between the transition state geometries, since the reacted trajectories tend to have orientations similar to the transition state geometries. Exceptions are found for the β, ϕ and γ angles for CH cleavage, where the initial angles cannot be close to the transition state geometries since a considerably large bend between the umbrella axis and the CO bond is required. Furthermore, for OH cleavage steering in the θ, β and α angles is observed during the reaction. This means that effectively the orientation of the OH bond relative to the rest of the molecule changes, while the geometry of the rest of the molecule does not change. For CH cleavage considerably more steering is observed than for OH cleavage, with steering in all angles but γ_1 and γ_2. In general, the initial angular distribution for OH cleavage is comparable to the initial angular distribution of scattered trajectories, while this is not the case for the angular distribution for CH cleavage. It seems that dynamically the barrier for OH cleavage is more accessible than the barrier for CH cleavage, which is not only caused by the barrier height and bond length of the dissociating bond, but also due to the large bend between the umbrella and the CO bond that is required for CH cleavage. Finally, the angle of the CO bond w.r.t. the surface normal is the most important angle for determining whether OH or CH cleavage will occur.

G. Formation of formaldehyde

All reacted trajectories have been propagated for an additional 200 fs after a bond was broken. Some of these trajectories show formation of formaldehyde, for which the probability is provided in Figure 9. Here we see that increasing the incidence energy leads to

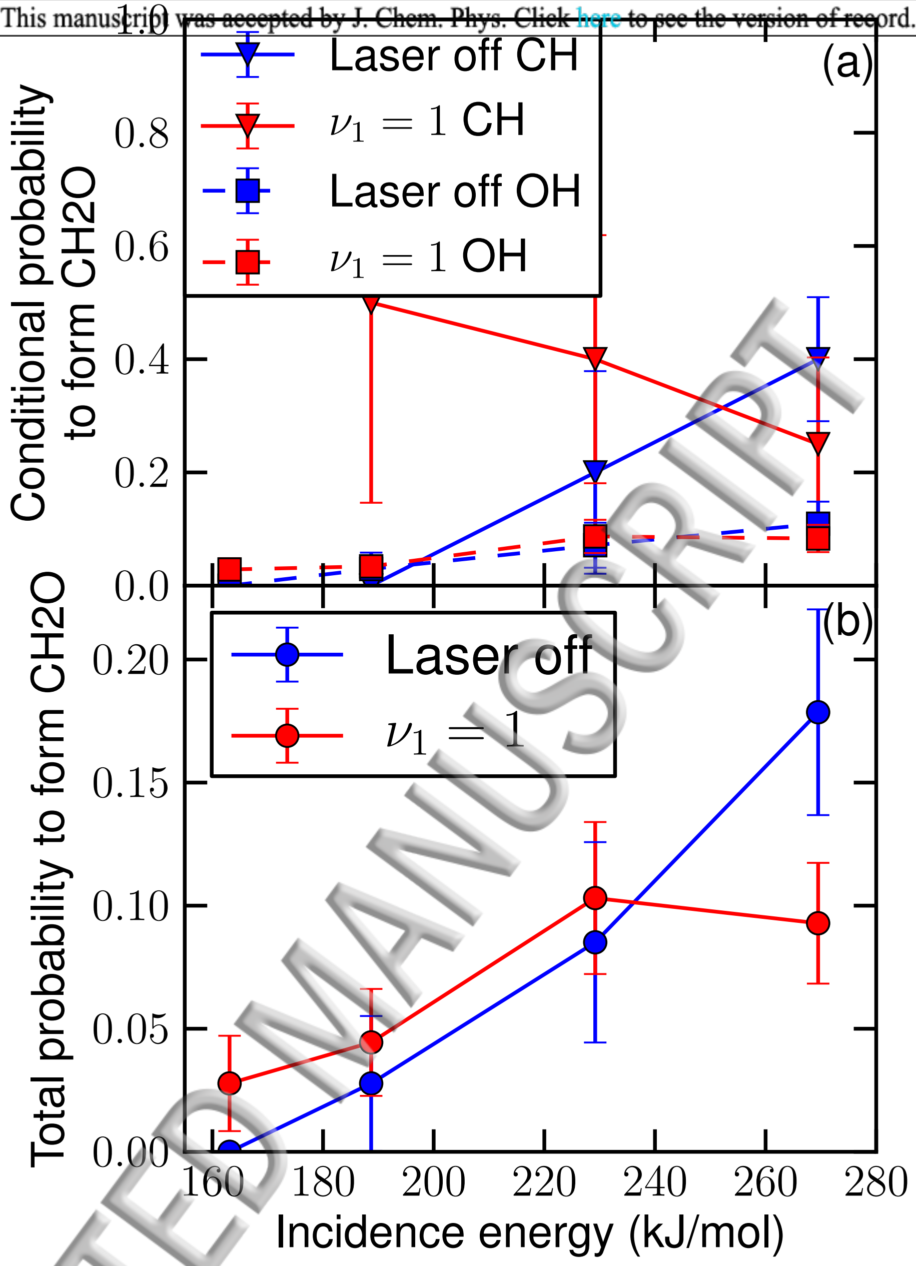

Figure 9. Probability to form formaldehyde within 200 fs after the first bond is broken for laser off (blue) and $\nu_1 = 1$ (green) AIMD simulations at various incidence energies. Panel a shows the conditional probability to form formaldehyde for when either the CH (solid lines) or the OH bond (dashed) is broken first, while panel b shows the total probability. The error bars represent 68% confidence intervals.

increased formaldehyde formation. This is probably caused by more energy remaining in the chemisorbed methanol or hot hydrogen after breaking the first bond, which results in a higher chance of breaking the second bond. Furthermore, if the CH bond is broken first, more formaldehyde formation is observed than when the OH bond is broken first. Thus, the increase of CH cleavage with $\langle E_i \rangle$ between 229 and 270 kJ/mol in the laser off prediction results in a sharp increase of formaldehyde formation, while this is not observed for $\nu_1 = 1$, for which CH cleavage is initially suppressed. Interestingly, previously it was expected that the dominant pathway would be via breaking the OH bond first[9], whereas here we see that it is dependent on the kinetic energy. At low energies "OH cleavage first" is the dominant pathway, while at high energies "CH cleavage first" becomes the dominant pathway. Moreover, increasing the $\langle E_i \rangle$ from 229 to 270 kJ/mol with $\nu_1 = 1$ does not increase formaldehyde formation, instead about 1% recombinative desorption of methanol is observed at $\langle E_i \rangle = 270$ kJ/mol. Also, the conditional probability for laser off at the highest energy is about 10% as well, suggesting that the conditional probability limit to form formaldehyde after breaking first the OH bond is about 10%.

Three mechanisms for formaldehyde formation have been observed. The first mechanism involves a hot hydrogen traveling along the surface, and abstracting another hydrogen atom from the dissociated methanol resulting in formaldehyde and molecular hydrogen, after which both desorb from the surface. The second mechanism also involves a hot hydrogen traveling along the surface, but kinetic energy is transferred from the hot hydrogen to the dissociated methanol once the hydrogen gets close. This results then in formaldehyde and two atomic hydrogens. Both mechanisms suffer from the supercell size, where effectively the hot hydrogen interacts with a periodic image. However, this may not be a large issue if we would consider this example to represent a methanol coverage of 1/12th of a monolayer. The third mechanism does not suffer from this periodic problem, since it involves two bonds to break simultaneously or subsequently, which again results in formaldehyde and atomic hydrogen. Furthermore, only two trajectories resulted in a product where two CH bonds were broken, with no clear relation to the incidence energy or vibrational excitation. Moreover, one of the two trajectories recombined again to CH_2OH. Although these theoretical predictions are for low coverage, experimental evidence exists for formaldehyde forming from methanol at high pressure, and thus high coverage, as well[48,49]. Finally, independent of mechanism, formaldehyde is observed to desorb rapidly after formation due to the relatively low barrier for desorption, which is also observed experimentally[49–51].

IV. CONCLUSIONS

Predictions for the reactivity of methanol on Cu(111) are made using AIMD, supported with an analysis of barriers and elbow plots. It is shown that Cu(111) is highly selective in breaking the OH bond due to the difference in barrier heights and dynamical features of the MEPs for OH and CH cleavage. Moreover, the vibrational efficacy of the OH stretch mode for dissociative chemisorption of methanol is high and vibrationally exciting this mode suppresses CH cleavage. Furthermore, additional insight is gained into the reaction mechanism following dissociative chemisorption of methanol by propagating reacted trajectories further. Within a short timescale (200 fs) formaldehyde formation was observed, for which experimental evidence exists. Three different mechanisms for this formaldehyde production are identified, where two mechanisms involve a hot hydrogen that either abstracts another hydrogen forming molecular hydrogen or knocks off another hydrogen resulting in two atomic hydrogens at the surface. In the third mechanism, the OH and CH bond are broken simultaneously or subsequently. In general, the probability of formaldehyde production is higher at higher incidence energy, and if a CH bond is broken first instead of breaking an OH bond first. Finally, we hope that our theoretical predictions will be followed by experiments in order to test the transferability of the SRP32-vdW functional among similar systems.

SUPPLEMENTARY MATERIAL

See supplementary material for more detailed procedures and results for the AIMD.

ACKNOWLEDGMENTS

This work has been financially supported by the European Research Council through an ERC2013 advanced grant (Nr. 338580) and through an NWO/CW TOP Grant (Nr. 715.017.001). Furthermore, this work was carried out on the Dutch national e-infrastructure with the support of NWO-EW.

REFERENCES

[1]S. Sá, H. Silva, L. Brandão, J. M. Sousa, and A. Mendes, Applied Catalysis B: Environmental **99**, 43 (2010).

[2]J. N. Russell, S. M. Gates, and J. T. Yates, Surface Science **163**, 516 (1985).

[3]A. Chen and R. Masel, Surface Science **343**, 17 (1995).

[4]M. Bowker, Topics in Catalysis **3**, 461 (1996).

[5]Z.-T. Wang, Y. Xu, M. El-Soda, F. R. Lucci, R. J. Madix, C. M. Friend, and E. C. H. Sykes, The Journal of Physical Chemistry C **121**, 12800 (2017).

[6]D. Mei, L. Xu, and G. Henkelman, The Journal of Physical Chemistry C **113**, 4522 (2009).

[7]X.-K. Gu and W.-X. Li, The Journal of Physical Chemistry C **114**, 21539 (2010).

[8]Z.-J. Zuo, L. Wang, P.-D. Han, and W. Huang, International Journal of Hydrogen Energy **39**, 1664 (2014).

[9]R. Garcıá-Muelas, Q. Li, and N. López, ACS Catalysis **5**, 1027 (2015).

[10]Z. Jiang, B. Wang, and T. Fang, Applied Surface Science **364**, 613 (2016).

[11]S.-S. Wang, X.-K. Gu, H.-Y. Su, and W.-X. Li, The Journal of Physical Chemistry C **122**, 10811 (2018).

[12]W. Chen, E. D. Cubuk, M. M. Montemore, C. Reece, R. J. Madix, C. M. Friend, and E. Kaxiras, The Journal of Physical Chemistry C **122**, 7806 (2018).

[13]J. Chen, X. Zhou, Y. Zhang, and B. Jiang, Nature Communications **9**, 4039 (2018).

[14]B. A. Peppley, J. C. Amphlett, L. M. Kearns, and R. F. Mann, Applied Catalysis A: General **179**, 31 (1999).

[15]Y. Choi and H. G. Stenger, Applied Catalysis B: Environmental **38**, 259 (2002).

[16]J. K. Lee, J. B. Ko, and D. H. Kim, Applied Catalysis A: General **278**, 25 (2004).

[17]S. Patel and K. K. Pant, Chemical Engineering Science **62**, 5425 (2007).

[18]G.-J. Kroes, Physical Chemistry Chemical Physics **14**, 14966 (2012).

[19]B. Jackson, F. Nattino, and G.-J. Kroes, The Journal of Chemical Physics **141**, 054102 (2014).

[20]J. Wellendorff, T. L. Silbaugh, D. Garcia-Pintos, J. K. Nørskov, T. Bligaard, F. Studt, and C. T. Campbell, Surface Science **640**, 36 (2015).

[21]S. Gautier, S. N. Steinmann, C. Michel, P. Fleurat-Lessard, and P. Sautet, Physical Chemistry Chemical Physics **17**, 28921 (2015).

[22] G.-J. Kroes, The Journal of Physical Chemistry Letters **6**, 4106 (2015).

[23] F. Nattino, D. Migliorini, G.-J. Kroes, E. Dombrowski, E. A. High, D. R. Killelea, and A. L. Utz, The Journal of Physical Chemistry Letters **7**, 2402 (2016).

[24] D. Migliorini, H. Chadwick, F. Nattino, A. Gutiérrez-González, E. Dombrowski, E. A. High, H. Guo, A. L. Utz, B. Jackson, R. D. Beck, and G.-J. Kroes, The Journal of Physical Chemistry Letters **8**, 4177 (2017).

[25] H. Chadwick, A. Gutiérrez-González, D. Migliorini, R. D. Beck, and G.-J. Kroes, The Journal of Physical Chemistry C (2018), 10.1021/acs.jpcc.8b05887.

[26] G. Kresse and J. Hafner, Physical Review B **49**, 14251 (1994).

[27] G. Kresse and J. Hafner, Physical Review B **47**, 558 (1993).

[28] G. Kresse and J. Furthmüller, Physical Review B **54**, 11169 (1996).

[29] G. Kresse and J. Furthmüller, Computational Materials Science **6**, 15 (1996).

[30] G. Kresse and D. Joubert, Physical Review B **59**, 1758 (1999).

[31] P. E. Blöchl, Physical Review B **50**, 17953 (1994).

[32] M. Methfessel and A. T. Paxton, Physical Review B **40**, 3616 (1989).

[33] G. Henkelman and H. Jónsson, The Journal of Chemical Physics **111**, 7010 (1999).

[34] A. Heyden, A. T. Bell, and F. J. Keil, The Journal of Chemical Physics **123**, 224101 (2005).

[35] J. Kästner and P. Sherwood, The Journal of Chemical Physics **128**, 014106 (2008).

[36] P. Xiao, D. Sheppard, J. Rogal, and G. Henkelman, The Journal of Chemical Physics **140**, 174104 (2014).

[37] A. Mondal, M. Wijzenbroek, M. Bonfanti, C. Díaz, and G.-J. Kroes, The Journal of Physical Chemistry A **117**, 8770 (2013).

[38] F. Nattino, H. Ueta, H. Chadwick, M. E. van Reijzen, R. D. Beck, B. Jackson, M. C. van Hemert, and G.-J. Kroes, The Journal of Physical Chemistry Letters **5**, 1294 (2014).

[39] N. Gerrits, D. Migliorini, and G.-J. Kroes, The Journal of Chemical Physics **149**, 224701 (2018).

[40] B. Hammer, L. B. Hansen, and J. K. Nørskov, Physical Review B **59**, 7413 (1999).

[41] J. P. Perdew, K. Burke, and M. Ernzerhof, Physical Review Letters **77**, 3865 (1996).

[42] M. Dion, H. Rydberg, E. Schröder, D. C. Langreth, and B. I. Lundqvist, Physical Review Letters **92**, 246401 (2004).

[43] R. A. Marcus, The Journal of Chemical Physics **45**, 4493 (1966).

[44]E. A. McCullough and R. E. Wyatt, The Journal of Chemical Physics **51**, 1253 (1969).

[45]D. A. King and M. G. Wells, Proc. R. Soc. Lond. A **339**, 245 (1974).

[46]B. Baule, Annalen der Physik **349**, 145 (1914).

[47]F. O. Goodman and H. Y. Wachman, "Formula for thermal accommodation coefficient," Tech. Rep. (Defense Technical Information Center, Fort Belvoir, VA, 1966).

[48]N. Takezawa and N. Iwasa, Catalysis Today **36**, 45 (1997).

[49]T. Shishido, Y. Yamamoto, H. Morioka, and K. Takehira, Journal of Molecular Catalysis A: Chemical **268**, 185 (2007).

[50]C. Barnes, P. Pudney, Q. Guo, and M. Bowker, Journal of the Chemical Society, Faraday Transactions **86**, 2693 (1990).

[51]J. Greeley and M. Mavrikakis, Journal of Catalysis **208**, 291 (2002).

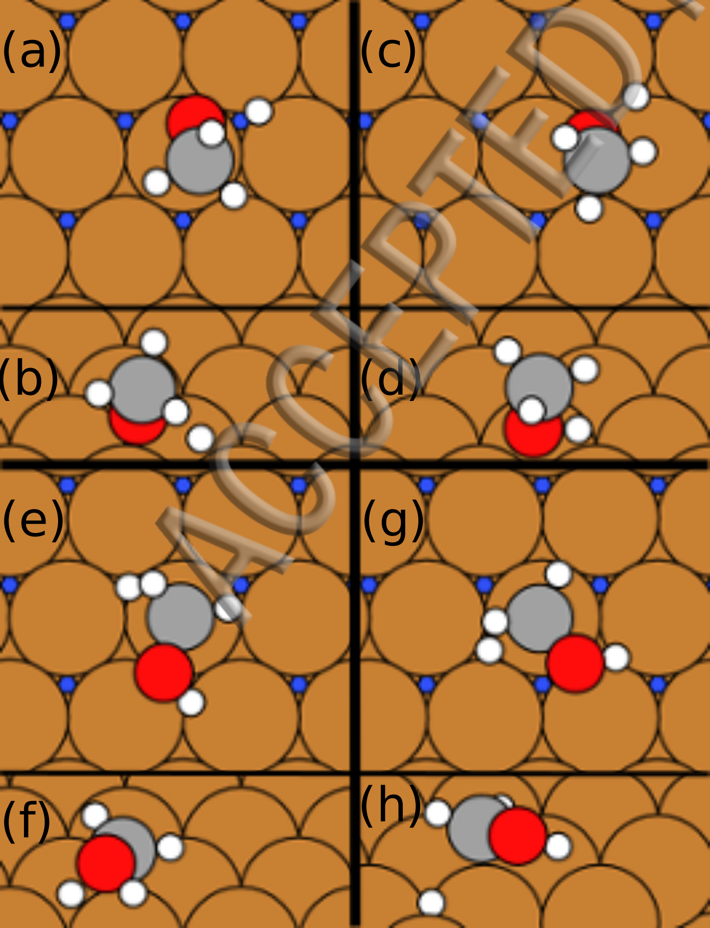

ACCEPTED

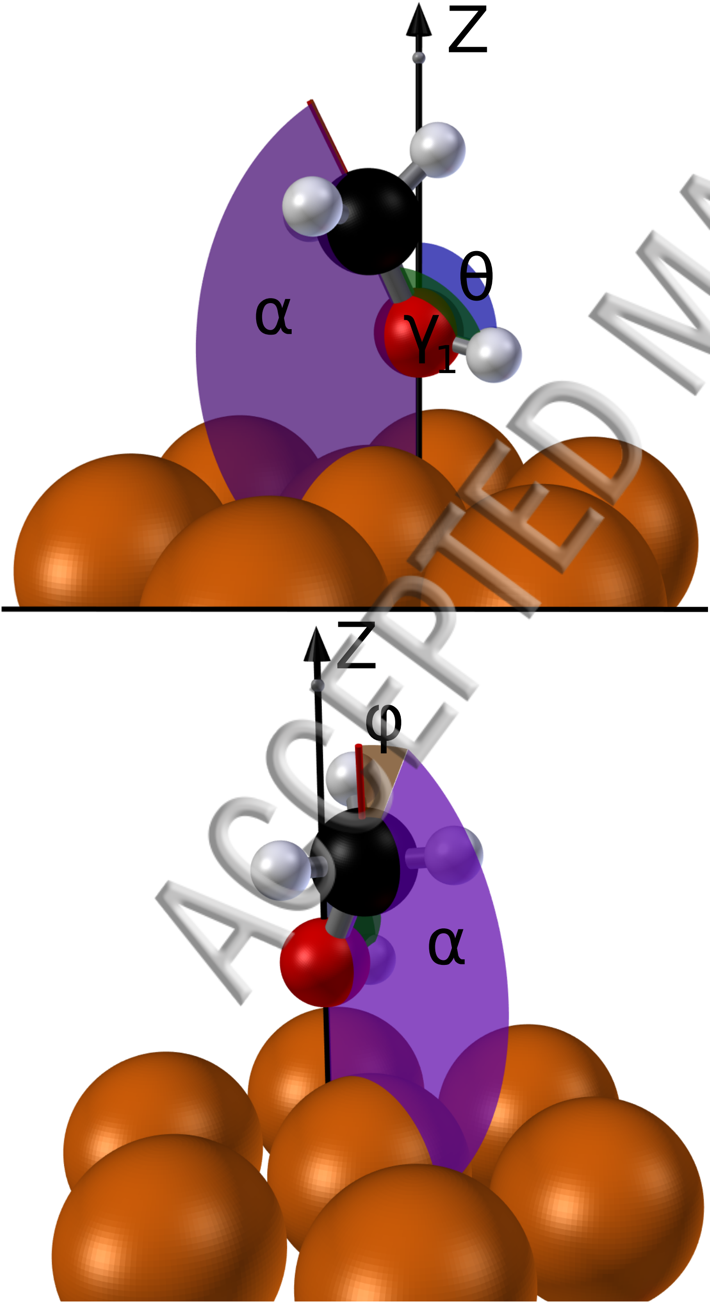

ACCEPTED M

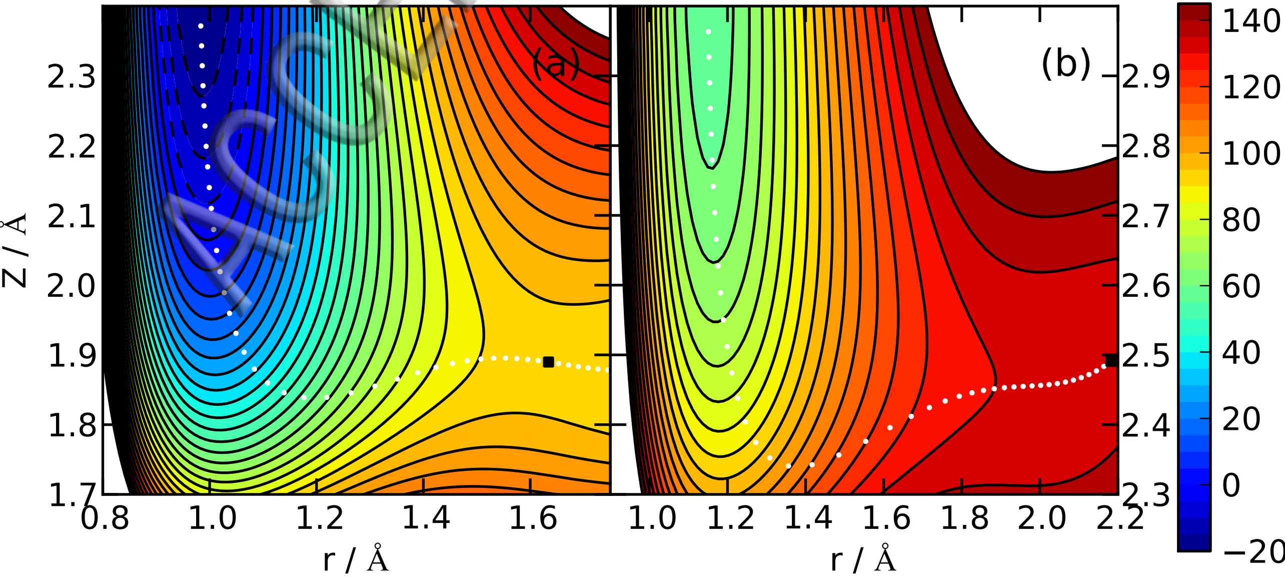
(a)
(b)
Z / Å
2.3
2.2
2.1
2.0
1.9
1.8
1.7
0.8
1.0
1.2
1.4
1.6
r / Å
2.9
2.8
2.7
2.6
2.5
2.4
2.3
1.0
1.2
1.4
1.6
1.8
2.0
2.2
r / Å
140
120
100
80
60
40
20
0
−20

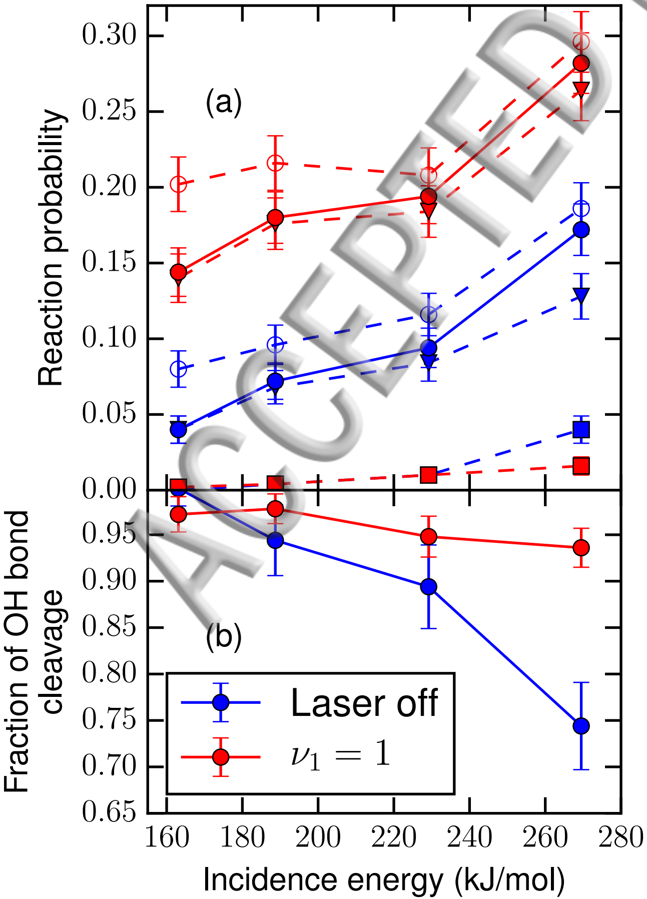
(a)
Reaction probability
0.00
0.05
0.10
0.15
0.20
0.25
0.30
(b)
Fraction of OH bond cleavage
0.65
0.70
0.75
0.80
0.85
0.90
0.95
Laser off
$\nu_1 = 1$
160
180
200
220
240
260
280
Incidence energy (kJ/mol)
ACCEPTED

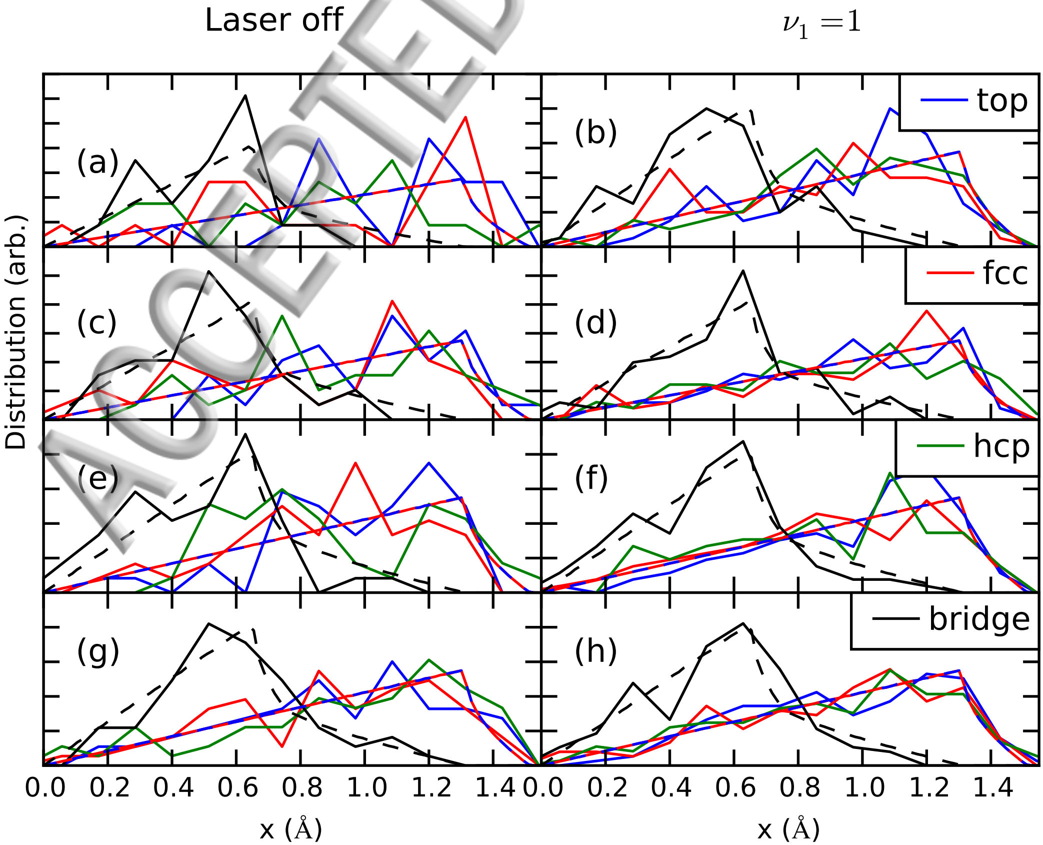
Laser off
$\nu_1 = 1$
top
fcc
hcp
bridge
(a)
(b)
(c)
(d)
(e)
(f)
(g)
(h)
Distribution (arb.)
0.0 0.2 0.4 0.6 0.8 1.0 1.2 1.4
0.0 0.2 0.4 0.6 0.8 1.0 1.2 1.4
x (Å)
x (Å)

ACCEPTED

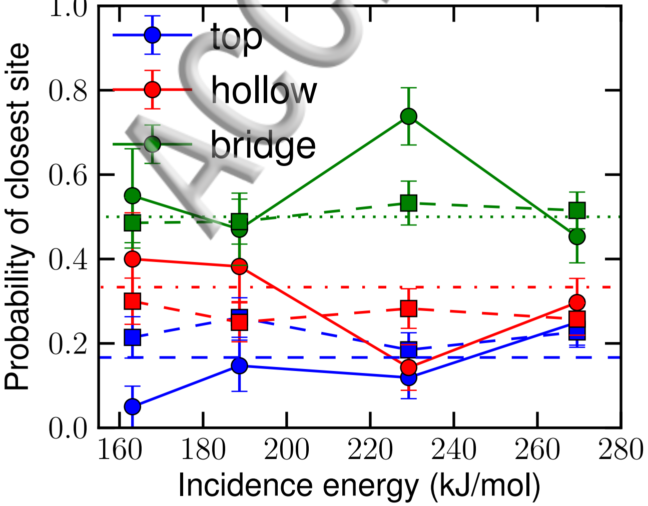
top
hollow
bridge
Probability of closest site
0.0
0.2
0.4
0.6
0.8
1.0
160
180
200
220
240
260
280
Incidence energy (kJ/mol)

ACC

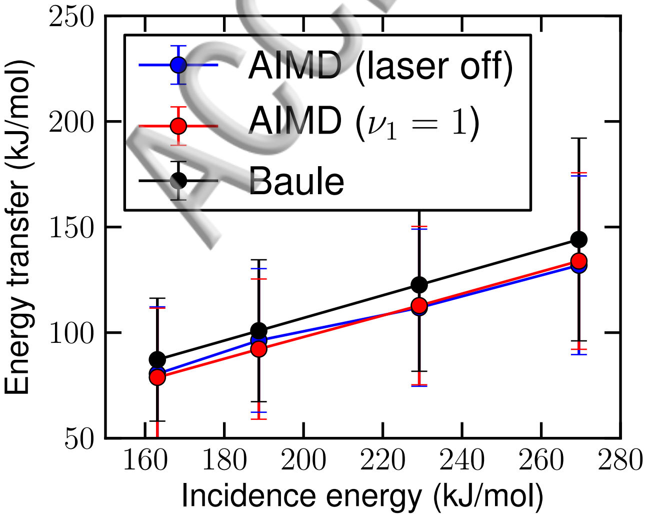

AIMD (laser off)
AIMD ($\nu_1 = 1$)
Baule
Energy transfer (kJ/mol)
Incidence energy (kJ/mol)
250
200
150
100
50
160
180
200
220
240
260
280

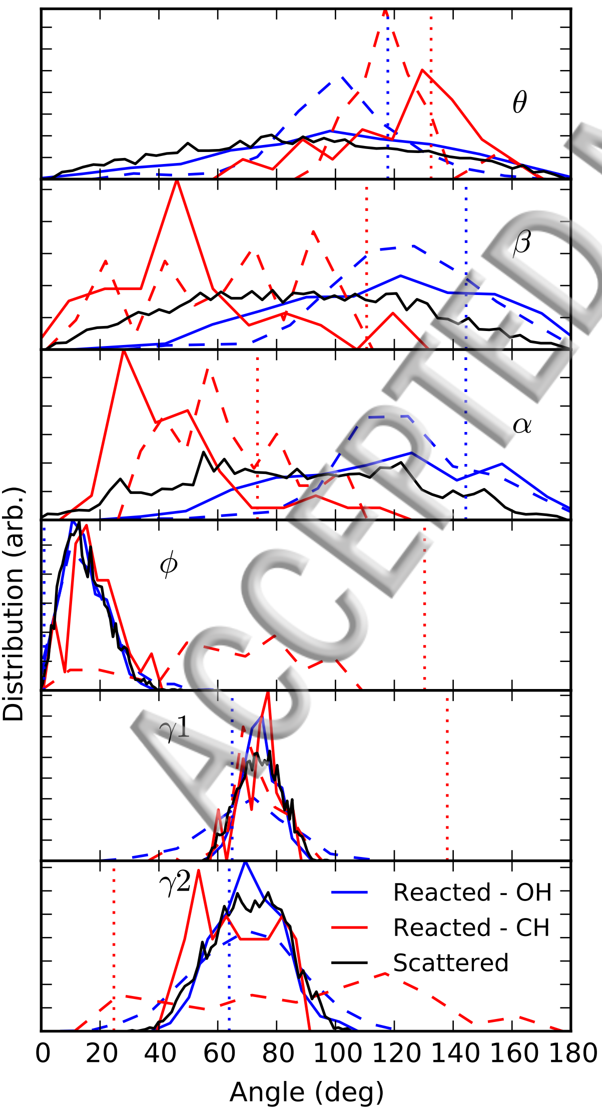
θ
β
α
φ
γ1
γ2
Reacted - OH
Reacted - CH
Scattered
Distribution (arb.)
0
20
40
60
80
100
120
140
160
180
Angle (deg)

ACCEPTED M

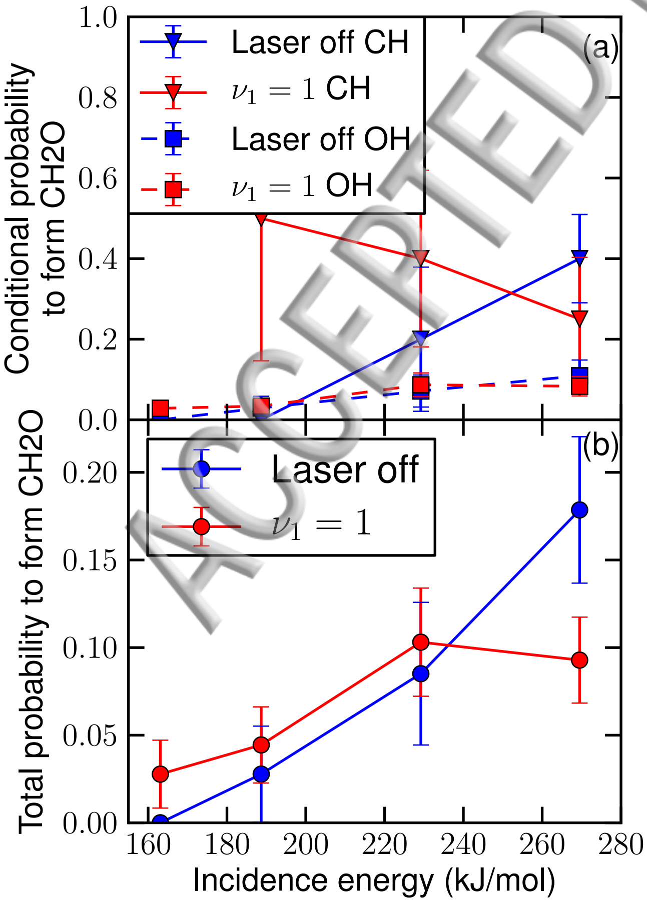

(a)
Conditional probability to form CH2O
Laser off CH
$\nu_1 = 1$ CH
Laser off OH
$\nu_1 = 1$ OH
1.0
0.8
0.6
0.4
0.2
0.0
(b)
Total probability to form CH2O
Laser off
$\nu_1 = 1$
0.20
0.15
0.10
0.05
0.00
160
180
200
220
240
260
280
Incidence energy (kJ/mol)

ACCEPTED